HTD-Vol. 206-3, Topics in Heat Transfer – Volume 3
ASME 1992

UNSTEADY SOLIDIFICATION IN MICROGRAVITY

Branko Kosovic and George S. Dulikravich
Pennsylvania State University
University Park, Pennsylvania

ABSTRACT

We have developed a mathematical model and an accompanying computer program for the computational simulation of an unsteady laminar flow of an incompressible fluid undergoing solidification. An extended Boussinesq approximation allowing for temperature-dependent physical properties of the fluid was used. Latent heat of phase change was incorporated via an enthalpy method. A single computer code thus simultaneously predicts unsteady velocity, pressure and temperature fields in the thermally buoyant melt while capturing the advancing solid front. The same code can simulate the reverse process of unsteady thawing or melting of the solid phase.

INTRODUCTION

In controlled freezing processes [1] it is very important to fully understand the solid accretion since the accumulated solid effectively reduces and deforms the cross sectional area of the passages and causes significant local variations in pressure and flow field shear stresses. Eventually, the solid phase completely fills the passage at certain locations thus blocking the main flow and creating isolated pockets of undercooled fluid. Further freezing of this fluid creates significant residual stresses in the frozen material. During the freezing or thawing process, secondary flows are generated due to strong buoyancy forces. It has been shown [2-4] that a magnetic field can eliminate vorticity from the melt flow field, while an electric field can enhance it [5].

In this work we have not incorporated the magnetic and electric fields. Instead, we have formulated the entire problem as time-dependent and three-dimensional, although our computational results will be for two-dimensional situations only.

ANALYTICAL MODEL

The entire set of conservation law partial differential equations can be non-dimensionalized by introducing the relations

$$v_i^* = \frac{v_i}{v_o} \qquad x_i^* = \frac{x_i}{l_o}$$
$$t^* = \frac{t\, v_o}{l_o} \qquad p^* = \frac{p}{\rho_o\, v_o^2} \tag{1}$$
$$\Phi^* = \frac{\Phi}{\eta_o\, v_o^2/l_o^2} \qquad g^* = \frac{g_i}{g}$$
$$\theta = \frac{\Delta T}{\Delta T_o} \qquad e^* = \frac{e}{c_{po}\, \Delta T_o} \tag{2}$$

where T_c is the temperature of the cold wall and T_h is the temperature of the hot wall, so that $\Delta T = T - T_c$, and $\Delta T_o = T_h - T_c$. The symbols v_o, l_o, ρ_o, η_o, c_{po} designate reference values of melt velocity, length, density, dynamic viscosity, and specific heat, respectively. In addition, local values of pressure, internal energy of the melt, and linear acceleration are designated with p, e, and g, respectively. Non-dimensionalization results in the following non-dimensional groups

Reynolds number $$Re = \frac{\rho_o v_o l_o}{\eta_o}$$

Froude number $$Fr^2 = \frac{v_o^2}{g\, l_o}$$

Grashof number $$Gr = \frac{\rho_o^2\, \alpha\, g\, l_o^3\, \Delta T_o}{\eta_o^2}$$

Eckert number $$Ec = \frac{v_o^2}{c_{po}\, \Delta T_o}$$

Prandtl number $$Pr = \frac{\eta_o\, c_{po}}{k_o} \qquad (3)$$

Here, k_o is the reference value of heat conductivity and α is the coefficient of thermal expansion. Fluid density and coefficients of specific heat, viscosity and heat conduction can be expressed as general functions of temperature [6,4]:

$$\rho = \rho_o\, \rho'(\theta) \quad c_p = c_{po}\, c_{po}'(\theta) \quad c_v = c_{vo}\, c_{vo}'(\theta) \qquad (4)$$

$$\eta = \eta_o\, \eta'(\theta) \quad k = k_o\, k'(\theta) \qquad (5)$$

where the primed values denote functions of non-dimensional temperature, θ. The non-dimensional density ρ' can be expanded in a Taylor series while retaining only the first order term

$$\rho' = 1 - \alpha\, \Delta T = 1 - \alpha^*\, \theta \qquad (6)$$

where

$$\alpha^* = \frac{\partial \rho'}{\partial \theta} = \frac{\Delta T_o\, \rho_o\, \partial \rho'}{\Delta T_o\, \partial \rho}$$

expansion, α, is constant in the range of temperatures which are of interest in a particular case. When the term $(\Delta T_o\, \alpha) \ll 1$, equations more general than what is known as the Boussinesq approximation can be derived for the fluid with non-constant properties [6,4].

In the case of solidification or melting the substantial derivative of the enthalpy per unit mass of the mushy region becomes

$$\frac{dh}{dt} = c_p \frac{dT}{dt} + L \frac{dS}{dt} \qquad (8)$$

where L is the latent heat (enthalpy of solid/liquid phase change) and S is the volumetric fraction of the solid phase. Then

$$v_i\, h_{,i} = c_p\, v_i\, T_{,i} - L\, v_i\, S_{,i} = \left(c_p - L\, S_{,T}\right)\, v_i\, T_{,i} \qquad (9)$$

where a comma designates a partial derivative.

Let $c_{pe} = c_p - L\, S_{,T}$ be an equivalent specific heat so that

$$c_{pe} = c_{po}\, c_{pe}' = c_{po} \left(c_p' - \frac{L\, S_{,\theta}\, \theta_{,T}}{c_{po}}\right) \qquad (10)$$

where S could be an arbitrary function of θ and c_{pe}' is the non-dimensional equivalent specific heat. This approach is called the "enthalpy method" [7]. It should be pointed out that the viscous dissipation, $\Phi^{(i)}$, can be neglected [3,4] when using the Boussinesq approximation since

$$\frac{\rho_o\, c_{pe}\, \frac{\partial T}{\partial t}}{\Phi^{(i)}} = \frac{Re}{Ec} \gg 1 \qquad (11)$$

The combination of non-dimensional hydrostatic, hydrodynamic, and magnetic pressures is

$$\tilde{p} = p + \frac{\phi}{Fr^2} \qquad (12)$$

where ϕ is the non-dimensional gravity potential defined as $g_i = \phi_{,i}$.

$$\frac{\partial}{\partial\theta} \quad \frac{\rho_o}{\Delta T_o}\frac{\partial}{\partial\theta} \quad \frac{\rho_o}{\partial T} \quad -\Delta T_o\alpha \qquad (7)$$

It can be assumed that the coefficient of thermal

The conservation laws in non-dimensional form then become [5]

$$v_{i,i} = 0 \tag{13}$$

$$v_{i,t} + (v_i v_j)_{,j} = \frac{1}{Re}(\eta' v_{i,j})_{,j} - p_{,i} + \frac{Gr\,\theta}{Re^2} g_i \tag{14}$$

$$\theta_{,t} + v_i \theta_{,i} = \frac{1}{RePr\, c_{pe}'}(k' \theta_{,i})_{,i} \tag{15}$$

NUMERICAL ALGORITHM

The non-dimensional conservative form of the three-dimensional Navier-Stokes equations for incompressible flows can be expressed in generalized (ξ, η, ζ) curvilinear non-orthogonal boundary-conforming coordinates as

$$\frac{\partial \bar{Q}}{\partial t} + \frac{\partial \bar{E}}{\partial \xi} + \frac{\partial \bar{F}}{\partial \eta} + \frac{\partial \bar{G}}{\partial \zeta} = D^2 + \bar{S} \tag{16}$$

where $\bar{Q}$ is the solution vector and $\bar{E}$, $\bar{F}$ and $\bar{G}$ are the flux vectors. The transformed source vector is denoted by $\bar{S}$. The viscous diffusion term in general curvilinear coordinates is

$$D^2 = \left(\frac{\bar{C}}{J} g_{ij} (J\bar{Q})_{,j}\right)_{,i} \tag{17}$$

where $J = \frac{\partial(\xi,\eta,\zeta)}{\partial(x,y,z)}$ is the Jacobian determinant of the geometric transformation from physical Cartesian coordinates (x, y, z) into the curvilinear non-orthogonal boundary-conforming (ξ, η, ζ) computational space. The metric tensor is defined as

$$g_{ij} = \frac{\partial \bar{x}_i}{\partial \hat{x}_j} \frac{\partial \bar{x}_j}{\partial \hat{x}_i} \tag{18}$$

while $\bar{x}_i$ is the Cartesian coordinate vector and $\hat{x}_i$ is the curvilinear coordinate vector:

$$\bar{x}_i = (x, y, z)^T \qquad \hat{x}_i = (\xi, \eta, \zeta)^T \tag{19}$$

Here, the superscript T represents a transpose. The contravariant components U, V, W of the melt velocity vector in the (ξ, η, ζ) computational space are related to the velocity components u, v, w in the Cartesian (x, y, z) coordinate system as follows

$$\begin{bmatrix} U \\ V \\ W \end{bmatrix} = \begin{bmatrix} \xi_x & \xi_y & \xi_z \\ \eta_x & \eta_y & \eta_z \\ \zeta_x & \zeta_y & \zeta_z \end{bmatrix} \begin{bmatrix} u \\ v \\ w \end{bmatrix} \tag{20}$$

For the Navier-Stokes equations, the generalized vectors are defined as

$$\bar{Q} = \frac{1}{J}\begin{bmatrix} \tilde{p}/\beta \\ u \\ v \\ w \\ \theta \end{bmatrix} \qquad \bar{E} = \frac{1}{J}\begin{bmatrix} U \\ Uu + \xi_x \tilde{p} \\ Uv + \xi_y \tilde{p} \\ Uw + \xi_z \tilde{p} \\ U\theta \end{bmatrix}$$

$$\bar{F} = \frac{1}{J}\begin{bmatrix} V \\ Vu + \eta_x \tilde{p} \\ Vv + \eta_y \tilde{p} \\ Vw + \eta_z \tilde{p} \\ V\theta \end{bmatrix} \qquad \bar{G} = \frac{1}{J}\begin{bmatrix} W \\ Wu + \zeta_x \tilde{p} \\ Wv + \zeta_y \tilde{p} \\ Ww + \zeta_z \tilde{p} \\ W\theta \end{bmatrix}$$

$$\bar{S} = \frac{Gr\theta}{Re^2 J}\begin{bmatrix} 0 \\ \tilde{e}_\xi \\ \tilde{e}_\eta \\ \tilde{e}_\zeta \\ 0 \end{bmatrix} \qquad \bar{C} = \frac{1}{Re}\begin{bmatrix} 0 \\ \eta' \\ \eta' \\ \eta' \\ \frac{k'}{Pr\, c_p'} \end{bmatrix}^T \tag{21}$$

The system of equations given by (21) is not hyperbolic since there is no physical time derivative term in the mass conservation equation. Consequently, the system cannot be integrated simultaneously. In order to integrate the system simultaneously and obtain a steady state solution, an artificial compressibility [8] term, $\frac{\partial}{\partial t}\left(\frac{\tilde{p}}{\beta J}\right)$, has been added to the mass conservation equation (13). Here, β is an artificial compressibility coefficient, a user specified parameter that depends on the problem geometry, grid, flow parameters, etc. [9]. In the steady state limit the

artificial compressibility term tends to zero. Thus, it does not influence the steady state solution.

TIME-ACCURATE RUNGE-KUTTA FOURTH ORDER EXPLICIT INTEGRATION

To obtain unsteady solutions of the Navier-Stokes equations using the artificial compressibility concept, it is common to use a dual time-stepping formulation. An explicit algorithm based on a Runge-Kutta scheme will be presented which is different than the common formulation [10,11] where the dual time-stepping was introduced in an implicit or semi-implicit mode. If an additional time (artificial time) is introduced, then the form of the Navier-Stokes equations suitable for obtaining a time-accurate numerical solution is

$$D\frac{\partial \vec{Q}}{\partial t} + \left(\frac{\partial \vec{Q}}{\partial \tau} + \frac{\partial \vec{E}}{\partial \xi} + \frac{\partial \vec{F}}{\partial \eta} + \frac{\partial \vec{G}}{\partial \zeta}\right) = D^2 + \vec{S} \qquad (22)$$

where τ represents the artificial time and D is a diagonal matrix defined as

$$D = \mathrm{diag}(0,1,1,1,1) \qquad (23)$$

The N-th order Runge-Kutta time-stepping method [12] given by

$$\begin{aligned} &\vec{Q}^0 = \vec{Q}^t \\ &\Delta\vec{Q}^n = -\alpha_n \Delta t\, \vec{R}^{n-1} \qquad n = 1,2,\ldots,N \qquad (24) \\ &\vec{Q}^{t+1} = \vec{Q}^t + \Delta\vec{Q}^N \end{aligned}$$

has been modified to introduce dual-time stepping. An inner loop over the artificial time, τ, has been applied only to the fourth stage of the Runge-Kutta algorithm. Thus,

$$\vec{Q}^0 = \vec{Q}^n \qquad (25)$$

where n = 3 is the index denoting the third stage of the outer loop in the physical time, t , of the fourth-order Runge-Kutta scheme, while k = 0 denotes the initial solution vector for the inner loop in the artificial time, τ. Then,

$$\vec{Q}^l\left[I + \alpha_l \frac{\Delta\tau}{\Delta t} D\right] = \vec{Q}^k - \alpha_l \Delta\tau\left[-\frac{1}{\Delta t} D\,\vec{Q}^n + \vec{R}^{l-1}\right]$$
$$l = 1,2,\ldots,L \qquad (26)$$

$$\vec{Q}^{n+1} = \vec{Q}^L$$

Since the dual time-stepping has been introduced only in the final stage of the outer loop in the physical time, t , it follows that

$$\vec{Q}^N = \vec{Q}^L \qquad (27)$$

Notice that the matrix $\left[I + \alpha_l \frac{\Delta\tau}{\Delta t} D\right]$ is diagonal and thus easily invertible. At the same time this means that the algorithm is explicit. The complete residual vector in the non-orthogonal curvilinear coordinates is defined as

$$\begin{aligned} \vec{R} = &\left[\frac{\partial \vec{E}}{\partial \xi} + \frac{\partial \vec{F}}{\partial \eta} + \frac{\partial \vec{G}}{\partial \zeta}\right]^l - \vec{S}^l \\ &- \frac{\varepsilon_2}{2J\Delta t}\left[\frac{\partial^2}{\partial \xi^2} + \frac{\partial^2}{\partial \eta^2} + \frac{\partial^2}{\partial \zeta^2}\right](J\vec{Q}^l) \\ &+ \frac{\varepsilon_4}{8J\Delta t}\left[\frac{\partial^4}{\partial \xi^4} + \frac{\partial^4}{\partial \eta^4} + \frac{\partial^4}{\partial \zeta^4}\right](J\vec{Q}^l) - (D^2)^l \end{aligned} \qquad (28)$$

where the overbars denote the vectors that were computed based on the solution vector $\vec{Q}$ in the artificial time, τ. The last two terms of the residual vector are the second and the fourth order artificial dissipation [12] where ε_2 and ε_4 are the user specified small parameters and Δt is the physical time step. For the four stage (K=4) Runge-Kutta method, the coefficients are α_k = 1/4, 1/3, 1/2 and 1, respectively. The explicit time integration scheme was used because it can be efficiently vectorized and because additional equations can be easily added to the system. The rate of convergence of explicit schemes is generally much lower than for implicit schemes, but when fully vectorized, these schemes need less central processor unit time to reach convergence than implicit schemes.

COMPUTATIONAL RESULTS

Based on this algorithm, a computer code has been developed for unsteady solidification in two dimensions.

Specifically, it was applied to the case of a closed rectangular container filled with molten steel that was cooled from above. Thus, the top of the container was suddenly subjected to a constant low temperature, while the bottom wall was kept at the high temperature. Both vertical walls were thermally insulated. A uniform computational grid consisted of 60x60 grid cells. Approximately 150 iterations ("time steps" $\Delta\tau$ with the artificial time) were needed per each physical time step, Δt , to achieve the desired accuracy. Values of the physical properties of the molten stainless steel and its solid phase are exposed in Table 1, while Table 2 contains nondimensional parameters. Table 3 contains values of parameters used in the numerical algorithm and in the non-dimensionalization. Computations were performed for two different values of gravitational acceleration. The first case represents solidification on the surface of the earth characterized with gravitational acceleration $g = 9.81\ m/s^2$, while the second case represents solidification in microgravity environment where the value of gravitational acceleration is reduced to only 0.01 g.

In the computed examples, it was assumed that all physical properties do not vary with temperature. Only viscosity was allowed to increase linearly with temperature between liquidus and solidus. Similarly, latent heat was assumed to be released linearly between the liquidus and the solidus temperatures.

A sequence of computer plots depict the computed evolution of the solid front and the molten steel flow field at the non-dimensional physical time levels of $t^* = 2,7,12,$ and 15, for the case including the gravity field characterized by $g = 9.81\ m/s^2$. Figures 1-8 depict isotherms, while figures 9-16 depict the velocity vector field. Figures 17 and 18 depict isotherms for the microgravity environment when the gravitational acceleration is reduced to 0.01g. This case had zero velocity field and therefore plots of velocity vector fields are not presented here. For the case with $g = 9.81\ m/s^2$ the entire evolution process was also captured on a video tape.

CONCLUSIONS

A complete analytical and numerical formulation has been developed for the prediction of unsteady solidification processes in fluid flows inside undercooled passages with or without the influence of a gravity field. Computational results confirm that gravity fields of different strength have a profound influence on the unsteady evolution of the solidifying flow field since they enhance flow recirculation and cause distorted patterns of the solidifying fronts. These changes are due to changes in the temperature field caused by free convection. Free convection occurs when the fluid (molten steel) is set into motion by inverting unstably stratified layers under the influence of a sufficiently strong gravity field. Convective heat transfer in the liquid layer influences heat transfer through the boundaries and consequently the amount of the solid phase accrued on undercooled walls. In the microgravity environment (0.01g) the fluid remains unstably stratified and the effect of convection is not present. Heat transfer in both liquid and solid layer is solely due to heat conduction.

The studies of the effect of gravity field when the container is differently oriented or rotated with respect to the gravity field have not been conducted. However, this can be a possible way to control the process of solidification.

ACKNOWLEDGMENTS

The authors would like to express their gratitude to Mr. Scott G. Sheffer for his help in the preparation of this paper. All computations and a video tape production were performed at Cray Research, Inc. in Eagan, Minnesota.

REFERENCES

1. Dulikravich, G.S., "Inverse Design and Active Control Concepts in Strong Unsteady Heat Conduction", *Applied Mechanics Reviews*, Vol. 41, No. 6, June 1988, pp. 270-277.

2. Lee, S. and Dulikravich, G. S., "Magnetohydrodynamic Steady Flow Computations in Three Dimensions", *International Journal for Numerical Methods in Fluids*, Vol. 13, No. 7, Oct. 1991a, pp. 917-936.; also AIAA Paper 91-0388, AIAA Aerospace Sciences Meeting, Reno, NV, Jan. 1991a.

3. Dulikravich, G. S., Kosovic, B. and Lee, S., "Solidification of Variable Property Melts in Closed Containers: Magnetic Field Effects", Proc. 13th IMACS World Congress on Computation and Applied Math., Dublin, Ireland, July 22-26, 1991.

4. Kosovic, B., Dulikravich, G.S. and Lee, S., "Freezing Under the Influence of a Magnetic Field: Computer Simulation", Proceedings of the 1991 ICHMT Int. Symp. on Heat and Mass Transfer in Biomed. Eng., Editors: K. Diller, A. Shitzer, S. Sideman, Athens, Geece, Sept. 2-6, 1991.

5. Lee, S., Dulikravich, G. S. and Kosovic, B., "Electrohydrodynamic (EHD) Flow Modeling and Computations", AIAA paper 91-1469, AIAA Plasma Physics, Fluid Dynamics and Lasers Conference, Honolulu, Hawaii, June 24-26, 1991b.

6. Gray, D. D., and Giorgini, A., "The Validity of the Bousinessq Approximation for Liquids and Gases", *International Journal of Heat and Mass Transfer*, Vol. 19, 1976, pp. 545-551.

7. Poirier, D., and Salcudean, M., "On Numerical Methods Used in Mathematical Modeling of Phase Change in Liquid Metals," ASME paper 86-WA/HT-22, The ASME Winter Annual Meeting, Anaheim, CA, December 7-12, 1986.

8. Chorin, A. J., "A Numerical Method for Solving Incompressible Viscous Flow Problems", *Journal of Computational Physics*, Vol. 2, 1967, pp. 12-26.

9. Lee, S. and Dulikravich, G.S., "Performance Analysis of DMR Method for Acceleration of Iterative Algorithms", AIAA paper 91-0241, AIAA Aerospace Sciences Meeting, Reno, NV, Jan. 7-10, 1991c.

10. Merkle, C. L., and Athavale, M., "Time-accurate Unsteady Incompressible Flow Algorithms Based on Artificial Compressibility," AIAA paper 87-1137, AIAA CFD Conference, Honolulu, Hawaii, June, 1987, pp. 397-407.

11. Breuer, M., and Hänel, D., "Solution of the 3-D, Incompressible Navier-Stokes Equations for the Simulation of Vortex Breakdown," Proceedings of the Eighth GAMM-Conference on Numerical Methods in Fluid Mechanics, Notes on Numerical Fluid Mechanics, Vol. 29, Ed. Pieter Wesseling

12. Jameson, A., Schmidt, W. and Turkel, E., "Numerical Solution of the Euler Equations by Finite Volume Methods Using Runge-Kutta Time-Stepping Scheme", AIAA paper 81-1259, AIAA Computational Fluid Dynamics Conference, Palo Alto, CA, June 1981.

ρ_o [kg m^{-3}]	6862
C_{pol} [J kg^{-1} K^{-1}]	788
C_{pos} [J kg^{-1} K^{-1}]	465.4 + 0.1336T
k_{ol} [W m^{-1} K^{-1}]	12.29 + 0.00325T
k_{os} [W m^{-1} K^{-1}]	8.116 + 0.01618T
T_l [K]	1727
T_s [K]	1670
η_o [kg m^{-1} s^{-1}]	6.5×10^{-3}
α [K^{-1}]	1.4×10^{-4}
L [J kg^{-1}]	265 200

TABLE 1. Physical Properties of Stainless Steel.

	g	0.01 g
Re	5278.46	5278.46
Ec	5.566×10^{-8}	5.566×10^{-8}
Pr	0.41676	0.41676
Gr	87.2426×10^{6}	87.2426×10^{4}

TABLE 2. Non-dimensional Numbers for Liquid Stainless Steel

β	1.0
CFL	2.8
ε	0.4
ε_2	0.0
ε_4	0.05
v_o	0.05 m s
l_o	0.1 m
ΔT_o	57 K
T_h	330.0 +T_c

TABLE 3. Numerical Algorithm Parameters

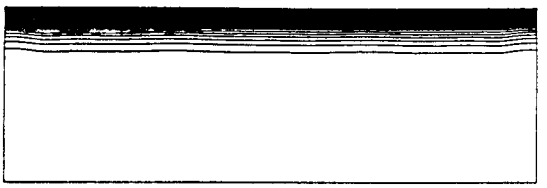

Figure 1. Isotherms for $t^* = 1$.

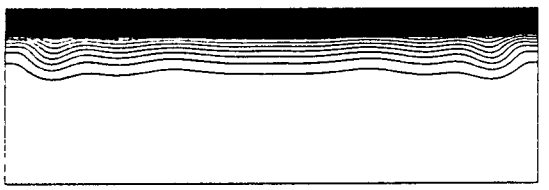

Figure 2. Isotherms for $t^* = 2$.

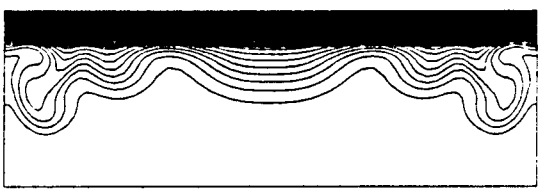

Figure 3. Isotherms for $t^* = 3$.

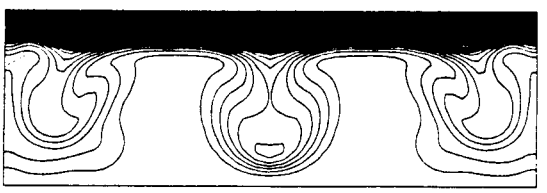

Figure 4. Isotherms for $t^* = 5$.

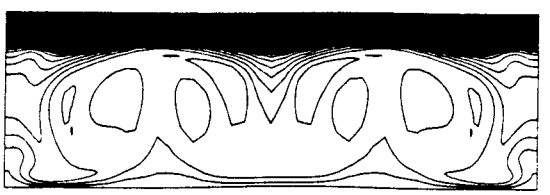

Figure 5. Isotherms for $t^* = 7$.

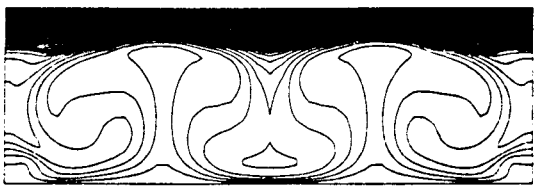

Figure 6. Isotherms for $t^* = 9$.

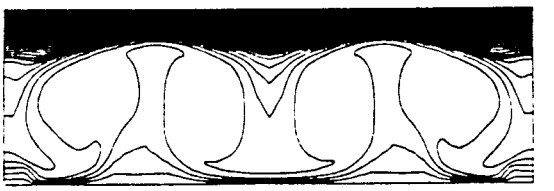

Figure 7. Isotherms for $t^* = 12$.

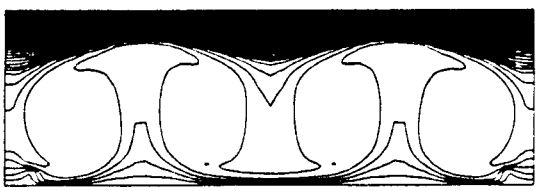

Figure 8. Isotherms for $t^* = 15$.

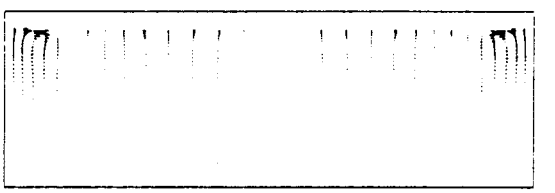

Figure 9. Velocity vector field for $t^* = 1$.

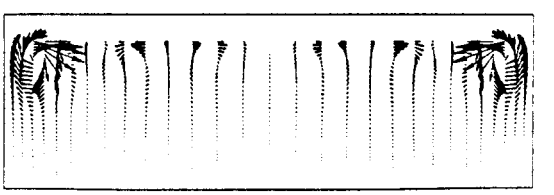

Figure 10. Velocity vector field for $t^* = 2$.

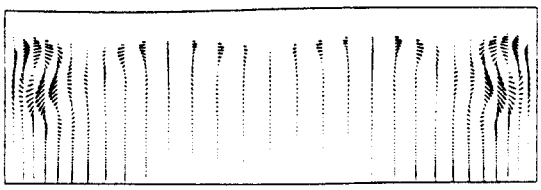

Figure 11. Velocity vector field for $t^* = 3$.

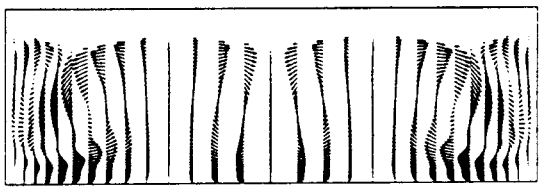

Figure 12. Velocity vector field for $t^* = 5$.

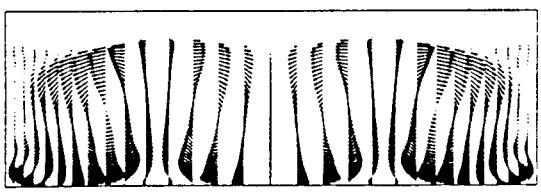

Figure 13. Velocity vector field for $t^* = 7$.

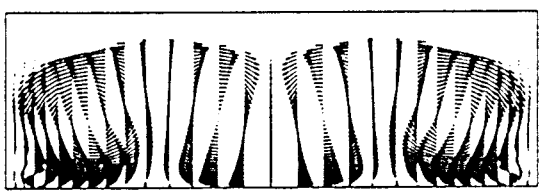

Figure 14. Velocity vector field for $t^* = 9$.

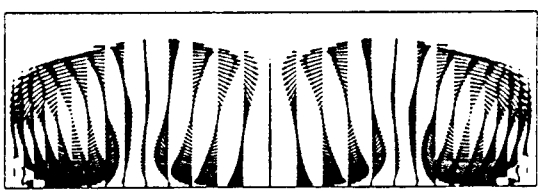

Figure 15. Velocity vector field for $t^* = 12$.

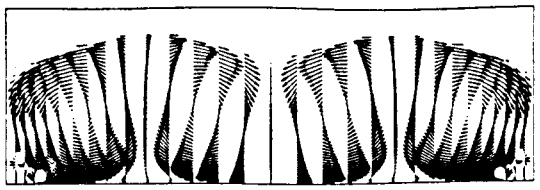

Figure 16. Velocity vector field for $t^* = 15$.

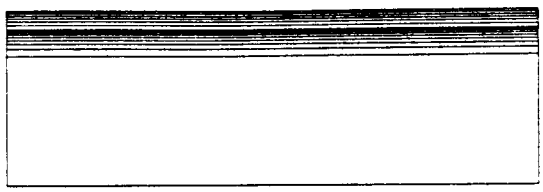

Figure 17. Isotherms for 0.01g $t^* = 1$.

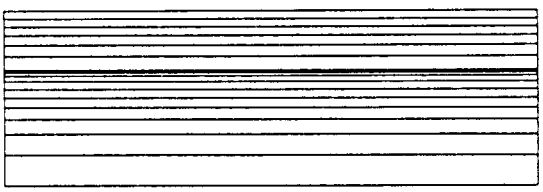

Figure 18. Isotherms for 0.01g $t^* = 15$.

HTD-Vol. 206–3

G. S. DULIKRAVIC

TOPICS IN HEAT TRANSFER

VOLUME III

- Microgravity Heat Transfer and Flow
- Heat Transfer in Space Energy Systems
- Nonconventional Heat Pipe Systems
- Heat Transfer in Thermal Insulation for Hypersonic Vehicles

presented at
THE 28TH NATIONAL HEAT TRANSFER CONFERENCE
AND EXHIBITION
SAN DIEGO, CALIFORNIA
AUGUST 9–12, 1992

sponsored by
THE HEAT TRANSFER DIVISION, ASME

edited by

R. S. DOWNING
SUNDSTRAND CORPORATION

K. VAFAI
OHIO STATE UNIVERSITY

L. HAAS
McDONNELL DOUGLAS
AIRCRAFT CORPORATION

W. S. CHANG
WRIGHT-PATTERSON A.F.B.

S. CHELLAIAH
FLORIDA INTERNATIONAL
UNIVERSITY

G. R. CUNNINGTON
LOCKHEED PALO ALTO
RESEARCH LABORATORY

E. E. ANDERSON
TEXAS TECH UNIVERSITY

THE AMERICAN SOCIETY OF MECHANICAL ENGINEERS
United Engineering Center • □ • □ • 345 East 47th Street • □ • □ • New York, N.Y. 10017